Post-Print

This is the accepted version of:

S. Meraglia, G. Gozzini, S. Liu, D. Invernizzi
Adaptive Control for High-Performance Trajectory Tracking in Multirotor UAVs
in: 9th International Conference on Control, Decision and Information Technologies (CoDIT'23), IEEE, 2023, ISBN: 9798350311402, p. 1-6 [9th International Conference on Control, Decision and Information Technologies (CoDIT'23), Roma, Italy, 3-6 July 2023]
doi:10.1109/CoDIT58514.2023.10284088

Adaptive control for high-performance trajectory tracking in multirotor UAVs

Salvatore Meraglia[1], Giovanni Gozzini[1], Shang Liu[1], Davide Invernizzi[1]

***Abstract*— This paper presents an adaptive position control law to achieve high-performance trajectory tracking in Unmanned Aerial Vehicles (UAVs). Considering a hierarchical control scheme, the main contribution of this work is the design of an adaptive augmentation of a baseline position controller to account explicitly for aerodynamic effects. The adaptive augmentation allows maintaining high-performance in situations where the baseline controller was not designed for or performs poorly. The results of experimental tests conducted using a small quadrotor are reported in order to compare the performance of the proposed design with respect to state-of-the-art non-predictive feedback controllers.**

I. Introduction

In recent years, the study of Unmanned Aerial Vehicles (UAVs) has received increasing attention thanks to their wide range of application. Several control designs have been proposed to track a predefined trajectory or a path for quadrotors. Fixed-gain linear or nonlinear controllers solve such problems satisfactorily when operating in nominal operations (see, *e.g.*, [1] for a comprehensive survey).

Advanced methods have been proposed to achieve high maneuverability, including Differential Flatness-Based Control (DFBC) [2] and Model Predictive Control (MPC) [3]. However, when facing external disturbances, achieving accurate tracking in an agile flight is still challenging [4]. In [5], Iterative Learning Control (ILC) was used to update the reference signal in multirotor systems subject to repetitive disturbances in order to achieve high-performance tracking. However, repetitive working conditions and controlled environments are essential for these data-based control algorithms. When increasing the flight speed, aerodynamic drag becomes the predominant disturbance [4]. Mathematically characterizing the aerodynamics of multirotor UAVs for control design purposes has been the focus of recent works [6], [7], [8]. In order to eliminate the negative effects caused by aerodynamic drag, a common practice is to adopt a feedforward compensation scheme (see, *e.g.*, [6], [2]). This compensation scheme typically relies on parameter identification techniques to obtain the drag coefficients. However, during the identification procedure, the rotor drag is assumed to be independent of the thrust. Since this assumption does not hold in reality, such a procedure leads to different drag coefficients on different trajectories where different thrust profiles are applied. To accurately capture complex aerodynamic effects, [9] proposes a hybrid approach that combines a rotor model based on Blade Element Momentum (BEM) theory with learned residual force and torque terms represented by a deep neural network. The main drawback of these identification approaches is the large amount of experimental data needed in the identification procedure.

To overcome this limitation, approaches capable of learning while operating are needed. Adaptive control is an attractive candidate to face the aforementioned disturbances and uncertainties for unmanned flight [10]. Model Reference Adaptive Control (MRAC) is one of the most widely known adaptive control techniques and there are many interesting results in the control of multirotor UAVs [11]. $\mathcal{L}_1$ adaptive control is another approach that has gained popularity in recent years due to its inherent ability to provide fast adaptation with guaranteed robustness [12]. Of note, $\mathcal{L}_1$ adaptive controllers have been successfully applied across various UAV applications (see, *e.g.*, [13], [14]).

Leveraging a hierarchical control scheme, the main contribution of this work is the design of an $\mathcal{L}_1$ adaptive augmentation of the position control system for a multirotor UAV taking explicitly into account aerodynamic effects and performance limitation of the attitude control system, which is not part of the adaptive design. The adaptive augmentation is intended to keep a high level of performance in situations where the baseline controller was not designed for or performs poorly. Simple design methods and low-cost online computations characterize the proposed method, which is important for real-time implementation, especially when on-board memory and computing capacity are limited. Experimental results[1] using a small quadrotor are provided to illustrate the performance of the proposed control design in representative scenarios and show the advantages with respect to a control law that compensates aerodynamic effects for using off-line identified parameters.

Notation. $\mathbb{R}\,(\mathbb{R}_{>0},\mathbb{R}_{\geq 0})$ denotes the set of (positive, nonnegative) real numbers, $\mathbb{R}^n$ denotes the n-dimensional Euclidean space and $\mathbb{R}^{m\times n}$ the set of $m\times n$ real matrices. The i-th vector of the canonical basis in $\mathbb{R}^n$ is denoted e_i and the identity matrix in $\mathbb{R}^{n\times n}$ is $I_n := [e_1 \cdots e_i \cdots e_n]$. Given vectors $x,y \in \mathbb{R}^n$, the standard inner product is defined as $\langle x,y\rangle := x^\top y$. The Euclidean norm of a vector $x\in\mathbb{R}^n$ is $|x| := \sqrt{\langle x,x\rangle}$. The n-dimensional unit sphere is denoted as $\mathbb{S}^n := \{x\in\mathbb{R}^{n+1} : |x|=1\}$. The set $\mathrm{SO}(3) := \{R\in\mathbb{R}^{3\times 3} : R^\top R = I_3, \det(R)=1\}$ is the 3D Special Orthogonal group. The map $S(\cdot):\mathbb{R}^3 \rightarrow$

[1]The Authors are with Dipartimento di Scienze e Tecnologie Aerospaziali, Politecnico di Milano, Via La Masa 34, 20156 Milano, Italy. Email addresses: shang.liu@mail.polimi.it, {giovanni.gozzini, salvatore.meraglia, davide.invernizzi}@polimi.it

This work was partially supported by the Italian Ministry for Research in the framework of the 2020 Program for Research Projects of National Interest (PRIN), under Grant 2020RTWES4.

[1]A video of an experiment showing the benefits of the adaptive augmentation can be watched at https://youtu.be/dzxYxpVT5Ns.

$\mathfrak{so}(3) := \{W \in \mathbb{R}^{3\times 3} : W = -W^\top\}$ is defined such that given $x, y \in \mathbb{R}^3$ one has $S(x)y = x \times y$. The inverse of S is denoted S^{-1}. Given a signal $x(t)$, $t \geq 0$, $x \in \mathbb{R}^n$, its $\mathcal{L}_\infty$ norm is defined as: $\|x\|_{\mathcal{L}_\infty} = \max_{i=1,..,n}\left(\sup_{\tau\geq 0}|x_i(\tau)|\right)$, where x_i is the i^{th} component of x.

II. Multirotor UAVs modeling including aerodynamic effects

Multirotor UAVs are flying platforms which consist of a central body and N arms, each of which carries a propeller. Let $\mathcal{F}_\mathcal{I} := (O_\mathcal{I}, \{x_\mathcal{I}, y_\mathcal{I}, z_\mathcal{I}\})$ be an inertial Cartesian frame and $\mathcal{F}_\mathcal{B} := (O_\mathcal{B}, \{x_\mathcal{B}, y_\mathcal{B}, z_\mathcal{B}\})$ be a body-fixed Cartesian frame attached to the center of mass of the multirotor, where $O_\mathcal{B}, O_I$ are the origins of the body and inertial frame, respectively. Defining $p \in \mathbb{R}^3$ as the position vector from O_I to $O_\mathcal{B}$, resolved in $\mathcal{F}_\mathcal{I}$, $R := \left[\begin{smallmatrix} b_1 & b_2 & b_3 \end{smallmatrix}\right] \in \mathrm{SO}(3)$ as the rotation matrix describing the attitude of $\mathcal{F}_\mathcal{B}$ with respect to $\mathcal{F}_\mathcal{I}$, the configuration of the UAV is fully described by the tuple $(p, R) \in \mathbb{R}^3 \times \mathrm{SO}(3)$.

When including aerodynamics effects, the nonlinear dynamical model of a multirotor UAV can be studied using the following set of equations [6]:

$$\dot{R} = RS(\omega) \tag{1}$$

$$J\dot{\omega} = -S(\omega)J\omega + \tau_c - D\omega - CR^\top v_a + \tau_e \tag{2}$$

$$\dot{p} = v \tag{3}$$

$$m\dot{v} = -mge_3 + \lambda T_c Re_3 - RAR^\top v_a - c_q v_a|v_a| - RB\omega + f_e, \tag{4}$$

where $J = J^\top \in \mathbb{R}^{3\times 3}_{>0}$, $m \in \mathbb{R}_{>0}$ is the UAV inertia matrix and mass, respectively, $g = 9.81\,\mathrm{m/s^2}$ is the gravitational acceleration, $\omega \in \mathbb{R}^3$ is the body angular velocity, $v \in \mathbb{R}^3$ is the inertial linear velocity, and $v_a = v - v_w$ represents the UAV velocity relative to the wind velocity $v_w \in \mathbb{R}^3$. The control inputs are $T_c > 0$ and $\tau_c \in \mathbb{R}^3$, which are the overall thrust and the torque applied by the propellers, respectively, and which depend upon the specific UAV configuration, whereas $(f_e, \tau_e) \in \mathbb{R}^6$ is the disturbance wrench. The term $\lambda \in \mathbb{R}_{>0}$ is an uncertain positive scalar representing the control effectiveness, which in nominal operating conditions (no fault) is slowly decreasing due to battery discharge, when this effect is not compensated by low-level controllers. As for the aerodynamic terms, the following contributions appear in the considered dynamic model: $A = \mathrm{diag}(a_x, a_y, a_z)$ is a linear velocity damping matrix associated with rotor drag, $B = bS(e_3)$ is a cross-coupling matrix associated with rotor flexibility, $D = \mathrm{diag}(d_x, d_y, d_z)$ is the angular velocity damping matrix, $C = cS(e_3)$ is a cross-coupling matrix proportional to the offset of the rotors with respect to $O_\mathcal{B}$, while c_q is the aerodynamic coefficient associated with the quadratic drag. We refer the reader to [6] for a thorough explanation on their derivation and on the underlying assumptions.

III. Control-oriented uncertain modeling and problem formulation

In this section we discuss the main approximations introduced in the dynamics to obtain a suitable control-oriented model, considering the same simplifications presented in [6] as far as aerodynamic modeling in concerned.

Assumption 1. *Given the dynamical model* (1)–(4)*, the following assumptions are considered:*

1) *There is no wind, i.e., $v_w = 0$.*
2) *The cross-coupling term in* (4) *associated with B is negligible, i.e., $B = 0$.*
3) *The linear damping term can be written as $A = c_\ell(I_3 - e_3 e_3^\top)$.*
4) *The angular velocity ω is considered as a control input.*

The first assumption is reasonable when working in indoor conditions. Nonetheless, the proposed control law will compensate exactly for constant wind gusts and will be able to deal with time-varying disturbances thanks to fast adaptation capabilities. Assuming $B = 0$ is instead equivalent to consider the rotors be rigid but such an assumption is reasonable also for flexible rotors, given that it is small in magnitude for small scale UAVs. When $A = c_\ell(I_3 - e_3 e_3^\top)$ (symmetric builds), the linear aerodynamic drag term in (4) simplifies to

$$RAR^\top v_a = c_\ell v_a - c_\ell(e_3^\top R^\top v_a)Re_3, \tag{5}$$

where the first term is independent of the attitude whereas the second one is directed along the thrust-axis Re_3, thereby appearing as a matched disturbance. Finally, the fourth assumption is widely adopted in the literature on control of multirotor UAVs [1]: given the full actuation capabilities of the attitude dynamics through τ_c and the fact that aerodynamic torques and cross-coupling terms are small in magnitude, the attitude dynamics can be controlled using classic designs, such as *PID* loops, that have been proven effective in handling also highly dynamic motions.

Hence, setting $\omega = \omega_c$ as the control variable for the attitude kinematics, we focus on the following control-oriented model:

$$\dot{R} = RS(\omega_c) \tag{6}$$

$$\dot{p} = v \tag{7}$$

$$m\dot{v} = -mge_3 + (\lambda T_c + c_\ell e_3^\top R^\top v)Re_3 - c_\ell v - c_q v|v| + f_e, \tag{8}$$

Setting $c_T := \lambda(1 - \lambda^{-1})$, we split the control thrust as $\lambda T_c = T_c + c_T T_c$. Then, to further simplify the design, we approximate the sum of nonlinear uncertain terms $(c_T T_c + c_\ell e_3^\top R^\top v)Re_3 + f_e$ with a vector of uncertain parameters $c_0 \in \mathbb{R}^3$, so that the velocity dynamics (8) becomes:

$$m\dot{v} = -mge_3 + T_c Re_3 + c_0 - c_\ell v - c_q v|v|. \tag{9}$$

We will exploit fast adaptation capabilities of the adaptive controller to handle the non-constant nature of c_0.

As we are addressing a trajectory tracking task, some basic assumptions on the smoothness and boundedness of the desired position trajectory are required to hold, consistently with those found in the literature [15].

Assumption 2. *Given a trajectory $t \mapsto (p_d(t), v_d(t)) \in \mathbb{R}^3 \times \mathbb{R}^3$, with $v_d(t) := \dot{p}_d(t)$, the following conditions hold:*

1) *the position trajectory $p_d(t)$ belongs at least to $\mathcal{C}^3$;*
2) *the acceleration $\dot{v}_d(t)$ and the jerk $\ddot{v}_d(t)$ are uniformly bounded in time;*
3) *the acceleration $\dot{v}_d(t)$ is such that* $\inf_{t\geq 0}|\dot{v}_{d_3}(t)-g|>0$.

Starting from these premises, the problem addressed in this work can be formalized as follows.

Problem 1. *Given the UAV uncertain model described by* (6), (7), (9), *design a control input $u=(T_c,\omega_c)\in\mathbb{R}_{>0}\times\mathbb{R}^3$ such that any position trajectory $t\mapsto(p_d(t),\dot{v}_d(t))\in\mathbb{R}^3\times\mathbb{R}^3$ satisfying Assumption 2 is practically asymptotically tracked.*

IV. Hierarchical control architecture

We approach the control design to solve Problem 1 using a hierarchical architecture to handle the underactuated nature of the multirotor model (1)–(4), which is based on the idea of controlling the attitude in such a way that the delivered force vector T_cRe_3 is aligned with the direction of the force required for position control [16]. Specifically, defining f_d as a desired control force to be designed for position tracking, a planned attitude $R_p\in\mathrm{SO}(3)$ is computed by assigning $R_pe_3=\frac{f_d}{|f_d|}=:b_{p_3}$ and by including a desired heading direction $b_{d_1}\in\mathbb{S}^2$ as a secondary control objective:

$$R_p:=\begin{bmatrix}\frac{b_{p_3}\times b_{d_1}}{|b_{p_3}\times b_{d_1}|}\times b_{p_3} & \frac{b_{p_3}\times b_{d_1}}{|b_{p_3}\times b_{d_1}|} & b_{p_3}\end{bmatrix}. \qquad (10)$$

Setting $T_c=|f_d|$ and then summing and subtracting $|f_d|R_pe_3$ from (9), we obtain the perturbed velocity dynamics

$$m\dot{v}=-mge_3+c_0-c_\ell v-c_qv|v|+f_d+\Delta f(R_p,R_e,f_d), \quad (11)$$

where $\Delta f:=(R_pR_eR_p^\top-I_3)f_d:=\Delta Rf_d$ represents the mismatch between the delivered force (aligned with b_3) and the desired force f_d, which depends upon the attitude error $R_e:=R_p^\top R$. Using (6), the dynamics of R_e is given by

$$\dot{R}_e=R_eS(\omega_c-R_e^\top\omega_p), \qquad (12)$$

with $\omega_p=S^{-1}(R_p^\top\dot{R}_p)$ being the planned angular velocity that can be computed analytically by time-differentiation of (10), given sufficiently smooth reference signals as per Assumption 2 (we assume constant heading direction set-point b_{d_1} in this work). Hence, the dynamics (7), (11), (12) takes then the form of a cascade system wherein the attitude error kinematics (12) perturbs the position dynamics (7), (11) through $\Delta f(R_p,R_e,f_d)$.

Given that the attitude error kinematics (12) is fully actuated by ω_c, we employ the rotation-matrix based law

$$\omega_c:=-\frac{1}{2}S^{-1}(K_RR_e-R_e^\top K_R)+R_e^\top\omega_p, \qquad (13)$$

where K_R is a gain matrix, which guarantees almost global asymptotic stability of the point $R_e=I_3$ provided that $\mathrm{tr}(K_R)I_3-K_R$ is positive definite [17].

V. Augmented adaptive control design

Focusing on the position dynamics, an augmented adaptive strategy is proposed to compensate for the considered uncertainties while ensuring asymptotic tracking. To this end, we decompose the control force as

$$f_d=m(\dot{v}_d+ge_3)+u, \qquad (14)$$

where $m(\dot{v}_d+ge_3)$ is a feedforward term compensating for the gravity and the desired acceleration and u is a feedback term to be designed. When plugging (14) into (11), one obtains

$$m\dot{v}=m\dot{v}_d+c_0-c_\ell v-c_qv|v|+u+\Delta f(R_p,R_e,f_d). \quad (15)$$

Then, defining the regressor matrix $\varphi(x_p):=\frac{1}{m}\begin{bmatrix}I_3 & -v & -|v|v\end{bmatrix}\in\mathbb{R}^{3\times5}$ and the vector of uncertain parameters $\theta:=\begin{bmatrix}c_0^\top & c_\ell & c_q\end{bmatrix}^\top\in\mathbb{R}^5$, the dynamics can be rewritten according to the standard linear-in-parameter form:

$$\dot{x}_p=A_px_p+B_p(u+\varphi(x_p)^\top\theta+\Delta f)+B_{pr}r \qquad (16)$$

where $x_p:=\begin{bmatrix}p^\top & v^\top\end{bmatrix}^\top$, $r:=\begin{bmatrix}p_d^\top & v_d^\top & \dot{v}_d^\top\end{bmatrix}^\top$, $A_p:=\begin{bmatrix}0 & I_3\\ 0 & 0\end{bmatrix}$, $B_p=\frac{1}{m}\begin{bmatrix}0\\ I_3\end{bmatrix}$, $B_{pr}:=\begin{bmatrix}0&0&0\\0&0&I_3\end{bmatrix}$. Finally, for adaptive augmentation, the feedback term u is split in a baseline $u_{b\ell}$ and an adaptive component u_{ad} as follows:

$$u=u_{b\ell}+u_{ad}. \qquad (17)$$

The augmented design allows one to leverage existing high-performance control laws designed on the nominal system while taking care of uncertain terms when operating far from the nominal conditions.

A. Baseline control design

PID-like control architectures are often employed in position control in multirotor UAVs, given their simplicity, ease of implementation and the availability of several systematic tuning methods. In this work, we select a PI law as the baseline controller:

$$\dot{x}_i=e_p \qquad (18)$$
$$u_{b\ell}=-K_Ix_i-K_Pe_p-K_De_v, \qquad (19)$$

where

$$e_p:=p-p_d, \qquad e_v:=v-v_d \qquad (20)$$

are the position and velocity errors, respectively, (18) represents the integrator dynamics while K_I, K_P and K_D are integral, proportional and derivative gain matrices, respectively. Defining the extended state $x_e:=\begin{bmatrix}x_i^\top & p^\top & v^\top\end{bmatrix}^\top\in\mathbb{R}^9$, the closed-loop position dynamics for the uncertainty-free system, obtained by substituting (19) into (11) with $\theta=0$, can be written as

$$\dot{x}_e=A_{ref}x_e+B_{ref}r+B_e\Delta f, \qquad (21)$$

where $A_{ref}:=\begin{bmatrix}0 & [I_3\ 0]\\ 0 & A_p\end{bmatrix}-\begin{bmatrix}0\\ B_p\end{bmatrix}\begin{bmatrix}K_I & K_P & K_D\end{bmatrix}=\begin{bmatrix}0 & I_3 & 0\\ 0 & 0 & I_3\\ -\frac{K_I}{m} & -\frac{K_P}{m} & -\frac{K_D}{m}\end{bmatrix}$, $B_{ref}:=\begin{bmatrix}-I_3 & 0 & 0\\ 0 & 0 & 0\\ \frac{K_P}{m} & \frac{K_D}{m} & I_3\end{bmatrix}$ and $B_e:=\begin{bmatrix}0\\ B_p\end{bmatrix}$.

The PI controller, combined with (13), guarantees local exponential tracking of the reference trajectory when referring to the uncertainty-free system. To show this, let us first write the closed-loop error dynamics for the uncertainty-free system:

$$\dot{R}_e = -\tfrac{1}{2} R_e (K_R R_e - R_e^\top K_R) \tag{22}$$

$$\dot{x}_i = e_p \tag{23}$$

$$\dot{e}_p = e_v \tag{24}$$

$$m\dot{e}_v = -K_I x_i - K_P e_p - K_D e_v + \Delta f(R_p, R_e, f_d(x_i, e_p, e_v)), \tag{25}$$

which is in the form of a cascade system with the perturbation term $\Delta f = \Delta R(R_p, R_e) f_d(x_i, e_p, e_v)$, that vanishes whenever $R_e = I_3$. Proving asymptotic tracking of a desired trajectory for the system (21)–(22), is then equivalent to show that $(R_e, x_i, e_p, e_v) = (I_3, 0, 0, 0)$ is an asymptotically stable equilibrium point for (22)–(25), which is claimed by the next theorem.

Theorem 1. *Let K_P, K_D, K_I be chosen such that A_{ref} is Hurwitz and K_R such that $tr(K_R)I_3 - K_R$ is positive definite. Then, the equilibrium point $(R_e, x_i, e_p, e_v) = (I_3, 0, 0, 0)$ is Locally Exponentially Stable (LES) for the system* (22)–(25).

Sketch of the Proof. Since $R_e = I_3$ is LES for (22) (see, *e.g.*, [17]) and the position subsystem is 0-GES (Globally Exponentially Stable) because A_{ref} is Hurwitz by assumption, namely, it is GES when $\Delta f \equiv 0$, then the equilibrium point $(R_e, x_i, e_p, e_v) = (I_3, 0, 0, 0)$ is LES by [18, Theorem 103]. Moreover, the cascade is well-defined, *i.e.*, R_p is always non-singular, because $f_{d_3}(t) > 0 \; \forall t \geq 0$ (hence $|b_{p_3}(t) \times b_{d_1}| \neq 0$ and $|f_d(t)| \neq 0 \; \forall t \geq 0$) when starting sufficiently close to the equilibrium point, thanks to item 3 of Assumption 2. □

B. Adaptive Augmentation design

In the following, we consider working under the assumption that $\Delta f \equiv 0$ (which vanishes as $t \to \infty$ since $R_e \to I_3$ according to (22)) for the purpose of deriving the adaptive component of the control law that solves the trajectory tracking problem in the uncertain case. Hence, we refer to the uncertain system:

$$\dot{x}_e = A_{ref} x_e + B_e (u_{ad} + \varphi^\top \theta) + B_{ref} r. \tag{26}$$

As mentioned in the Introduction, we select $\mathcal{L}_1$ adaptive control to ensure fast adaptation and to constrain the frequency content of the input u_{ad} to avoid sending too fast reference signals to the attitude controller, that could destabilize the system and is not part of the design for this work.

The adaptive control law is defined as follows:

$$\dot{\hat{x}}_e = A_{ref} \hat{x}_e + B_e \left(u_{ad} + \varphi^\top \hat{\theta} \right) + B_{ref} r + L\hat{e} \tag{27}$$

$$\dot{\hat{\theta}} = \Gamma_\theta \operatorname{Proj} \left(\hat{\theta}, \varphi B_e^\top P \hat{e} \right) \tag{28}$$

$$\dot{u}_{ad} = -\omega_f (u_{ad} + \varphi^\top \hat{\theta}) \tag{29}$$

where $\hat{e} := x_e - \hat{x}_e$ and $P = P^\top > 0$ is the solution of the Lyapunov equation $P(A_{ref} - L) + (A_{ref} - L)^\top P = -Q$ for some $Q = Q^\top > 0$. The tunable parameters are the adaptive gain matrix $\Gamma_\theta > 0$, the dissipation matrix $Q > 0$, the observer gain $L > 0$ and the cut-off frequency ω_f. For the system in (26) and the controller defined via (27)–(29), we have that[2]

$$(\|e_x\|_{\mathcal{L}_\infty}, \|e_v\|_{\mathcal{L}_\infty}) \propto \left(1/\Gamma_\theta, 1/\omega_f \right). \tag{30}$$

Based on (30), we can claim that the adaptive augmentation law solves Problem 1 for the position system (26). Increasing the bandwidth of the low-pass filter and the adaptation gain leads to small error bounds. However, low-pass filters with large bandwidths can generate high-gain feedback and thus lead to closed-loop systems with small robustness margins and susceptible to measurement noise. Indeed, the low-pass filter regulates the trade-off between performance and robustness.

VI. Results

This section presents the experimental tests performed to show and compare the behavior of the proposed control architecture with another state-of-the-art scheme. First, the procedure used to tune the controller parameters is explained, and then the results obtained in the experiments are shown.

A. Experimental Setup

Flight tests are performed inside the indoor Flying Arena for Rotorcraft Technologies (FlyART) of Politecnico di Milano which is equipped with a Motion Capture system (Mo-Cap) composed by 12 cameras. A fixed-pitch quadrotor designed by ANT-X [19] is used. The Mo-Cap system detects markers mounted on the UAV and collects measurements. The latter are received by a ground control station and forwarded to the drone (at a frequency of 100 Hz) along with the trajectory to be followed using specific waypoints (at a frequency of 20 Hz). Using the ANT-X rapid prototyping system for multirotor control, the control architecture is developed in Simulink and then integrated within the PX4 autopilot.

B. Control law tuning

The tuning of the gains of the baseline controller is carried out considering the mixed-sensitivity structured H_∞ synthesis [20] referring to the uncertainty-free model and using identified closed-loop linear models of the attitude dynamics [21]. As asymptotic trajectory tracking is already ensured by the baseline controller (Theorem 1), the synthesis focuses on the specification of performance with respect to a stabilization scenario, wherein the acceleration feedforward term is set to zero. Weighting functions in the frequency domain are used as control requirements for the synthesis. Specifically, two requirements are considered:

1) *Performance*: defined as a weighting function on the position sensitivity (transfer function from p_d to e_p).
2) *Control moderation*: defined as a weighting function on the control sensitivity (transfer function from p_d to u).

[2]This result holds if the $\mathcal{L}_1$-norm condition in [12, Equation 2.165] is satisfied. The interested reader is referred to [12] for the detailed derivation.

The inverses of the weighting functions on the sensitivity W_S and on the control sensitivity W_Q represent upper bounds on the corresponding frequency response magnitudes. The shape of W_S is chosen to achieve satisfactory stabilization performance while the shape of W_Q to avoid saturation, limiting the control action beyond the position dynamics bandwidth. The three main parameters to be chosen when shaping these two functions are the low frequency constraint (DC gain), the high frequency constraint (HF gain) and the cross-over frequency ω_{co} (directly related to the bandwidth). Then, the order n specifies how steep is the transition from low to high gain. In Table I, the parameters used to construct the n-th order weighting transfer functions with poles and zeros in a Butterworth pattern are reported.

TABLE I

PARAMETERS USED TO CONSTRUCT THE WEIGHTING FUNCTIONS FOR MIXED SENSITIVITY H_∞ SYNTHESIS.

	DC gain	ω_{co} [rad/s]	HF gain	Order n
W_S	10^{-5}	1	2	3
W_Q	10^{-5}	2	2.5	2

The following gains for (19) obtained from the tuning procedure are: $K_P = 0.377\, I_3$, $K_I = 0.129\, I_3$ and $K_D = 0.202\, I_3$. The parameters of the adaptive law(27)-(29) has been chosen as follows: $\Gamma_\theta = 100$, $\omega_f = 10\,\mathrm{rad/s}$, $L = 10$ and $Q = I_9$. The adaptation gain Γ_θ has been selected as high as possible considering the available on-board computing power, while the filter cut-off frequency ω_f is the result of the trade-off between performance and robustness by limiting interactions with the attitude dynamics. The attitude gain matrix $K_R = \mathrm{diag}(2.8, 2.8, 17.2)$ in (13) has been tuned by trial-and-error.

C. Flight experiments

In this section, we compare the results obtained by applying the proposed architecture with and without adaptive augmentation (denoted as *Adaptive* and *Baseline*, respectively) and the feedforward compensation scheme similar to [2], [22] (denoted as *Compensative*). Different scenarios are considered to evaluate the trajectory tracking performance using as metric the Root Mean Square position error (RMSE):

$$E_{tot} = \sqrt{\frac{1}{N}\sum_{k=1}^{N} E^k} \quad \text{with} \quad E^k = \|p^k - p_d^k\|^2 \qquad (31)$$

where N is the size of dataset collected during flights. Two test trajectories are considered: 1) Circle, *i.e.*, $p_d(t) = \begin{bmatrix}\sin(\Omega t) & \cos(\Omega t) & -1\end{bmatrix}^\top$ m with Ω ranging from 1 to $3.5\,\mathrm{rad/s}$,2) Eight, *i.e.*, $p_d(t) = \begin{bmatrix}0.5\sin(2\Omega t) & \cos(\Omega t) & -1\end{bmatrix}^\top$ m with Ω ranging from 1 to $2\,\mathrm{rad/s}$. In addition, to improve the validity of the result, each test is repeated three times, and the trial represented by the median E_{tot} is selected.

To apply the *Compensative* control law, we use the same parameters of the baseline controller and employ the drag coefficients identified running a Nelder-Mead optimization (as done in [2]) for which the quadrotor repeats a predefined trajectory (in this case a circle with $\Omega = 1\,\mathrm{rad/s}$) in each iteration of the optimization.

The comparison of the results is reported in Table II, highlighting the percentage improvements with respect the baseline controller alone in terms of RMSE (the $\times$ symbol indicates crashes during the experiments).

TABLE II

IN THIS TABLE THE RMSE IS SHOWN FOR DIFFERENT TRAJECTORIES AND VELOCITIES FOR THE THREE CONTROLLERS.

Trajectory	Ω [rad/s]	Baseline RMSE [m]	Compensative RMSE [m]	Compensative % ↓	Adaptive RMSE [m]	Adaptive % ↓
Circle	1	0.039	**0.019**	49	0.041	-6
Circle	1.5	0.087	**0.041**	53	0.058	33
Circle	2	0.170	0.112	34	**0.047**	72
Circle	2.5	0.294	0.205	30	**0.087**	70
Circle	3	0.338	0.268	21	**0.085**	75
Circle	3.5	$\times$	$\times$	$\times$	**0.132**	$\times$
Eight	1	0.045	0.050	-11	**0.041**	8
Eight	2	0.287	0.233	19	**0.169**	41

Inspecting the table, one can notice the performance improvements obtained by the approaches explicitly taking into account aerodynamic compensation (*Adaptive* and *Compensative*). The computed statistics show that trajectory tracking performance is significantly improved with the proposed adaptive approach when changing the trajectory used to identify the drag coefficient. Indeed, during the identification procedure, the rotor drag is assumed to be independent of the thrust. Since this assumption does not hold in reality, the identification procedure should be repeated for each different trajectory where different thrusts are applied.

We can see that the achieved performance is degraded when the desired trajectories, such as the Eight trajectory at $2\,\mathrm{rad/s}$, require fast attitude changes, which are tracked with an error by the attitude controller. Indeed, the attitude control law has been implemented without including the feedforward term ($\omega_p = 0$ in (13), as often done in practical implementations), and rely on a (given) inner-loop angular rate controller that in these challenging conditions might not perform so well, thereby violating the assumption $\omega = \omega_c$ (item 4 in Assumption 1). Instead, when the trajectories are too aggressive, such as the Circle at $3.5\,\mathrm{rad/s}$, the performance is degradated mostly by the actuation limits, as the commanded thrusts often hit the saturation bounds (Fig. 1). Of note, the *Adaptive* and *Compensative* approach were not able to complete the test in these conditions.

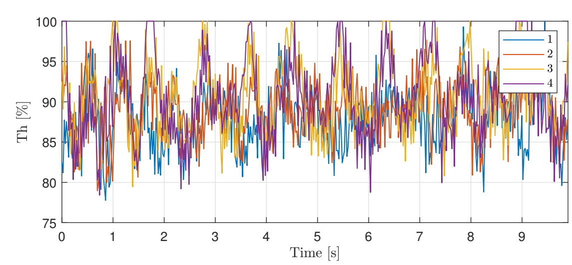

Fig. 1. Percentage of throttle for each motor during the circle trajectory at $3.5\,\mathrm{rad/s}$. It must be noted that the platform actuation limits are reached.

Due to space constraints only the results for circular trajectories with $\Omega = 3\,\mathrm{rad/s}$ are displayed. Specifically, in Fig. 2 the path in the *xy*-plane is shown, while in Fig. 3 the time evolution of the position error norm is depicted. Within the range of validity of the considered assumptions, the proposed approach effectively improves UAV tracking performance without requiring any off-line identification procedure.

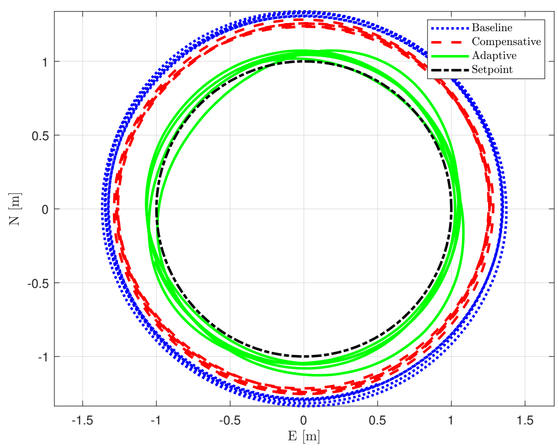

Fig. 2. In-plane position during a circular trajectory with $\Omega = 3\,\mathrm{rad/s}$.

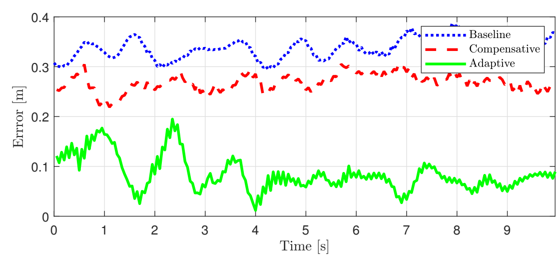

Fig. 3. Time evolution of the error norm during a circular trajectory with $\Omega = 3\,\mathrm{rad/s}$.

VII. Conclusions

We tackled the problem of high-performance trajectory tracking in multirotor UAVs for the solution of which an adaptive position controller based on $\mathcal{L}_1$ adaptive control has been developed. The main contribution is the design of an adaptive augmentation of a baseline position controller taking into account a simplified model of the aerodynamic effects. An experimental campaign involving a small quadrotor has shown the improvements of the proposed control architecture with respect to a state-of-the-art design based on an off-line identification procedure. Future work will address removing some of the simplifying assumptions outlined in Section II by including the attitude dynamics in the control design, with the objective of further improving performance and of deriving adaptive control laws with a larger domain of operating conditions.

References

[1] M.-H. Hua, T. Hamel, P. Morin, and C. Samson, "Introduction to feedback control of underactuated VTOL vehicles: A review of basic control design ideas and principles," *IEEE Control Systems Magazine*, vol. 33, no. 1, pp. 61–75, 2013.

[2] M. Faessler, A. Franchi, and D. Scaramuzza, "Differential flatness of quadrotor dynamics subject to rotor drag for accurate tracking of high-speed trajectories," *IEEE Robotics & Automation Letters*, vol. 3, no. 2, pp. 620–626, 2018.

[3] S. Sun, A. Romero, P. Foehn, E. Kaufmann, and D. Scaramuzza, "A Comparative Study of Nonlinear MPC and Differential-Flatness-Based Control for Quadrotor Agile Flight," *IEEE Transactions on Robotics*, vol. 38, no. 6, pp. 3357–3373, 2022.

[4] J. Jia, K. Guo, X. Yu, W. Zhao, and L. Guo, "Accurate high-maneuvering trajectory tracking for quadrotors: A drag utilization method," *IEEE Robotics & Automation Letters*, vol. 7, no. 3, pp. 6966–6973, 2022.

[5] S. Meraglia and M. Lovera, "Smoother-Based Iterative Learning Control for UAV Trajectory Tracking," *IEEE Control Systems Letters*, vol. 6, pp. 1501–1506, 2021.

[6] J.-M. Kai, G. Allibert, M.-D. Hua, and T. Hamel, "Nonlinear feedback control of quadrotors exploiting first-order drag effects," *IFAC-PapersOnLine*, vol. 50, no. 1, pp. 8189–8195, 2017, 20th IFAC World Congress.

[7] J. Svacha, K. Mohta, and V. Kumar, "Improving quadrotor trajectory tracking by compensating for aerodynamic effects," in *2017 international conference on unmanned aircraft systems (ICUAS)*. IEEE, 2017, pp. 860–866.

[8] M. Bangura, "Aerodynamics and control of quadrotors," Ph.D. dissertation, College of Engineering and Computer Science, The Australian National University, 2017.

[9] L. Bauersfeld, E. Kaufmann, P. Foehn, S. Sun, and D. Scaramuzza, "NeuroBEM: Hybrid Aerodynamic Quadrotor Model," in *2021 RSS Conference Robotics: Science and Systems*, 2021.

[10] P. Li, D. Liu, X. Xia, and S. Baldi, "Embedding adaptive features in the ardupilot control architecture for unmanned aerial vehicles," in *2022 IEEE 61st Conference on Decision and Control (CDC)*, 2022, pp. 3773–3780.

[11] Z. T. Dydek, A. M. Annaswamy, and E. Lavretsky, "Adaptive control of quadrotor UAVs: A design trade study with flight evaluations," *IEEE Transactions on Control Systems Technology*, vol. 21, no. 4, pp. 1400–1406, 2013.

[12] N. Hovakimyan and C. Cao, *$\mathcal{L}_1$ Adaptive Control Theory: Guaranteed Robustness with Fast Adaptation*. SIAM, 2010.

[13] H. Jafarnejadsani, D. Sun, H. Lee, and N. Hovakimyan, "Optimized $\mathcal{L}_1$ adaptive controller for trajectory tracking of an indoor quadrotor," *Journal of Guidance, Control, and Dynamics*, vol. 40, no. 6, pp. 1415–1427, 2017.

[14] G. Bressan, A. Russo, D. Invernizzi, M. Giurato, S. Panza, and M. Lovera, "Adaptive augmentation of the attitude control system for a multirotor UAV," *Journal of Aerospace Engineering*, vol. 234, no. 10, pp. 1587–1596, 2018.

[15] D. Invernizzi, M. Lovera, and L. Zaccarian, "Integral iss-based cascade stabilization for vectored-thrust uavs," *IEEE Control Systems Letters*, vol. 4, no. 1, pp. 43–48, 2020.

[16] D. Invernizzi, M. Lovera, and L. Zaccarian, "Dynamic attitude planning for trajectory tracking in thrust-vectoring UAVs," *IEEE Transactions on Automatic Control*, vol. 65, no. 1, pp. 453–460, 2020.

[17] D. Invernizzi, M. Lovera, and L. Zaccarian, "Hierarchical dynamic control for robust attitude tracking," *IFAC-PapersOnLine*, vol. 53, no. 2, pp. 6171–6176, 2020, 21st IFAC World Congress.

[18] M. Vidyasagar, *Nonlinear Systems Analysis (2nd Ed.)*. USA: Prentice-Hall, Inc., 1993.

[19] "ANT-X website." [Online]. Available: https://antx.it/

[20] P. Gahinet and P. Apkarian, "Structured H_∞ Synthesis in MATLAB," *IFAC Proceedings Volumes*, vol. 44, no. 1, pp. 1435–1440, 2011, 18th IFAC World Congress.

[21] D. Invernizzi, S. Panza, and M. Lovera, "Robust tuning of geometric attitude controllers for multirotor unmanned aerial vehicles," *Journal of Guidance, Control, and Dynamics*, vol. 43, no. 7, pp. 1332–1343, 2020.

[22] P. Foehn, D. Brescianini, E. Kaufmann, T. Cieslewski, M. Gehrig, M. Muglikar, and D. Scaramuzza, "Alphapilot: Autonomous drone racing," *Autonomous Robots*, vol. 46, no. 1, pp. 307–320, 2022.